Bidirectional visible light absorber based on nanodisk arrays

Qi Wang(王琦)[†], Fei-Fan Zhu(朱非凡), Rui Li(李瑞), Shi-Jie Zhang(张世杰), and Da-Wei Zhang(张大伟)

Engineering Research Centre of Optical Instrument and System, the Ministry of Education, Shanghai Key Laboratory of Modern Optical System, University of Shanghai for Science and Technology, Shanghai 200093, *China*

(Received 22 April 2022; revised manuscript received 23 June 2022; accepted manuscript online 19 August 2022)

A perfect bidirectional broadband visible light absorber composed of titanium nitride and tungsten nanodisk arrays is proposed. The average absorption of the absorber exceeds 89% at 400 nm–800 nm when light is normally incident on the front-side. Illumination from the opposite direction (back-side) results in absorption of more than 75%. Through the theoretical analysis of the electric and magnetic fields, the physical mechanism of the broadband perfect absorption is attributed to the synergy of localized surface plasmons, propagating surface plasmons, and plasmonic resonant cavity modes. Furthermore, the absorber also exhibits excellent polarization-independence performance and a high angular tolerance of $\sim 30^\circ$ for both front- and back-side incidence. The designed bidirectional broadband visible light absorber here has wide application prospects in the fields of solar cells and ink-free printing.

Keywords: bidirectional absorption, broadband absorber, polarization-independent, nanodisk arrays

PACS: 02.70.Bf, 02.60.Cb, 03.50.De **DOI:** 10.1088/1674-1056/ac8afa

1. Introduction

Recently, broadband absorbers have attracted much attention for their potential applications in sensing,[1] photo-thermovoltaics,[2] photodetection,[3] solar energy harvesting,[4,5] and so on. Many device configurations based on different materials and structures have been proposed to achieve these different applications. A simple method can be used to design perfect absorbers with flat film stacks, but the disadvantage is that it increases the manufacturing complexity due to multilayer film deposition.[6] Additionally, metamaterial-based surfaces[7,8] and metallic nanostructures employing surface plasmonic effects[9,10] have also been investigated to achieve superior optical absorbers. For example, Hedayati *et al.* presented a perfect absorber consisting of composite nanomaterial (Au/SiO_2) with almost 100% absorption, but it was designed with noble metal which increased the fabrication cost.[11]

In general, absorbers with metallic nanostructure are only probable to absorb light from the incident side.[12] Consider increasing absorption efficiency per unit area, Shen *et al.*[13] demonstrated an absorber based on a tapered dielectric nanostructure coated with a thin-layer of non-noble metal chromium on the substrate, which could yield bidirectional and polarization-independent absorption over 90% at the normal incidence, and 80% at a tilt incident angle of 60°. Therefore, the ideal absorber can not only absorb light from both sides of structure but also own high absorption efficiency with simple fabrication and low cost.

Here, we propose a bidirectional broadband absorber in the entire visible spectrum. The average absorption of the absorber exceeds 89% at 400 nm–800 nm when light is normally incident on the front-side. Illumination from the opposite direction (back-side) results in absorption of more than 75%. Firstly, based on the analysis of the electric and magnetic field distributions, the physical mechanism of the absorber is derived from the combined effect of local surface plasmon resonances (LSPRs), plasmonic resonant cavity (PRC) mode, and propagated surface plasmon resonances (PSPRs). Then, the influences of different nanodisk thicknesses on the absorption characteristics are studied. Finally, the absorption broadband characteristics keep almost the same at an oblique incident angle of up to 30° for both transverse magnetic (TM) and transverse electric (TE) polarizations, which may find potential applications in solar cells and ink-free printing.

2. Structure and method

The schematic of the visible broadband absorber is shown in Fig. 1(a). From top to bottom, the absorber is composed of the titanium nitride (TiN) nanodisk array ($h_1 = 150$ nm, $R_2 = 50$ nm) and tungsten (W) ($h_2 = 300$ nm, $R_1 = 75$ nm) nanodisk array at the top, W metal layer ($h_3 = 10$ nm) in the middle, and SiO_2 substrate ($h_4 = 90$ nm) at the bottom. The nanodisk array is symmetric in the x and y directions. Figure 1(b) is a cross-section of the metamaterial broadband absorber. The periods in the x and y directions are chosen as $\Lambda = 210$ nm. The metal at the bottom is not thick enough, so the absorption is calculated by using $A = 1 - R - T$,[14] where R represents reflection and T represents transmission. Here, the non-noble metal W is chosen as the metal material because W has good properties such as corrosion resistance and high-temperature resistance, which can be beneficial to the optical absorption. That is when the structure absorbs the visible light,

[†]Corresponding author. E-mail: shelly3030@163.com

© 2023 Chinese Physical Society and IOP Publishing Ltd

the temperature rises, W has good high-temperature stability. The refractive indexes of TiN, W, and SiO_2 are obtained from the data of Palik.[15]

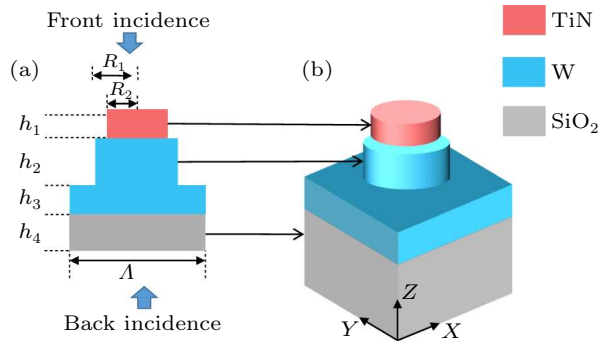


Fig. 1. Schematic design of structure (a) side view of the absorber, structural parameters: $\Lambda = 210$ nm, $h_1 = 150$ nm, $h_2 = 300$ nm, $h_3 = 10$ nm, $h_4 = 90$ nm, $R_1 = 75$ nm, and $R_2 = 50$ nm. (b) A structure diagram of the absorber.

In the simulation, the finite difference time domain (FDTD) method[16–19] is used to analyze the absorption performance of the absorber. The boundary conditions of the region along the x-axis and y-axis are periodic due to the symmetric structure, and the distance from the left to the right boundary is accurately equal to one period. The perfectly matched layer (PML) is used in the z-direction. The situation of the TM polarization (electric field along the x-axis) at normal incidence is studied, while the situation of the TE polarization is the same, which is incident along the positive and negative directions of the z-axis respectively. In addition, for oblique incidence, the BFAST plane wave is used. The mesh sizes of the x, y, and z directions are 2.5 nm × 2.5 nm × 2.5 nm, respectively.

3. Absorption performance analysis

The absorption spectra of the designed absorber in the front- and back-sided incidence under the TM polarization is shown in Fig. 2. It is evident that the absorptivity is greater than 89% in the visible band from 400 nm to 800 nm in the front-sided case. In addition, the absorptivity is greater than 75% in the back incidence. The average absorptivity is calculated as $A = \int_{\lambda_2}^{\lambda_1} A(\lambda)\mathrm{d}\lambda/(\lambda_1 - \lambda_2)$,[20] where λ_1 is 400 nm and λ_2 is 800 nm. Therefore, according to the formula, the average absorptivity in this wavelength range reaches 92.7% in the front-sided case and 83.5% in the back incidence.

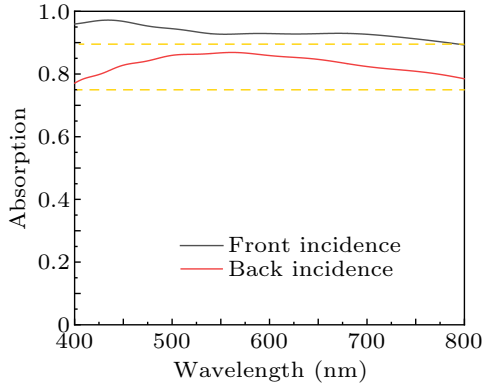


Fig. 2. Absorption spectra of structures in the front- (black) and back-sided (red) incidence.

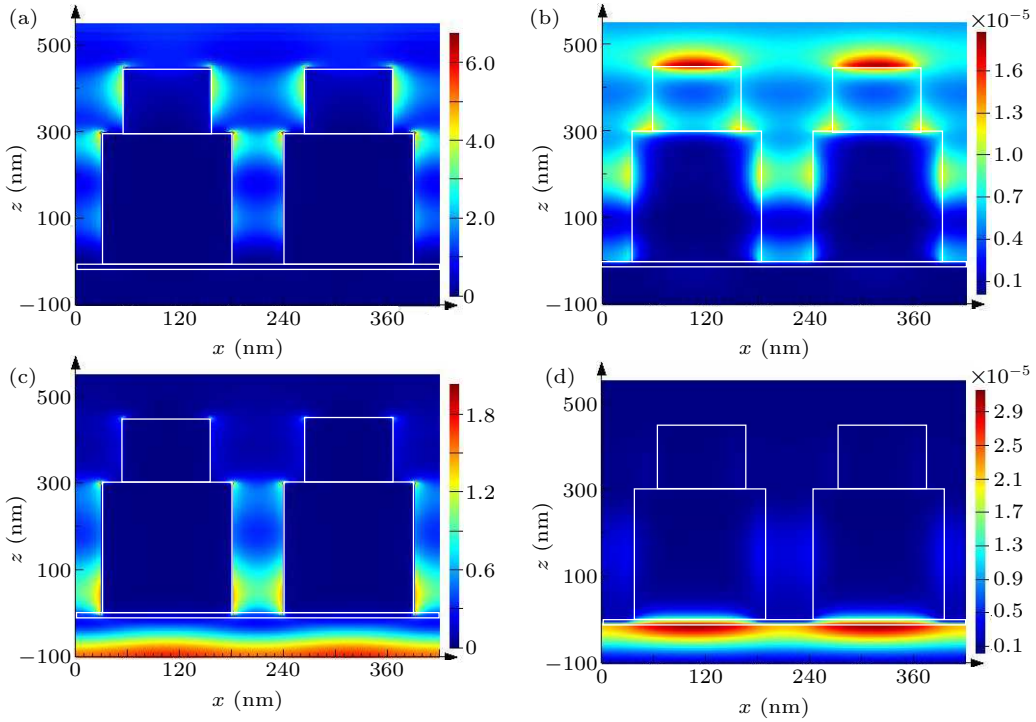


Fig. 3. Panels (a) and (b) are the electric and magnetic field distributions in the x–z plane when resonance wavelength $\lambda = 431$ nm and $y = 105$ nm in the front-sided incidence. Panels (c) and (d) are the electric and magnetic field distributions in the x–z plane when resonance wavelength $\lambda = 566$ nm and $y = 105$ nm in the back incidence. The white lines are the structural contour and represent two periods. The parameters are the same as those in Fig. 1.

To reveal the physical mechanism of the absorber, the electric and magnetic field distributions at the absorption peak wavelength $\lambda = 431$ nm in the front-sided incidence and $\lambda = 566$ nm in the back-sided case are illustrated, respectively. Figures 3(a) and 3(b) are the electric and magnetic field distributions at 431 nm under the TM polarization, respectively. White lines represent the outline of the structure, distinctly showing the structure of two periods. As can be seen in Fig. 3, the electric field is 5 orders of magnitude larger than that of the magnetic field, indicating that the electric field enhancement plays a leading role in broadband absorption.[21] In Fig. 3(a), the enhanced electric field mainly concentrates on the left and right edges of the upper part of TiN nanodisks as well as the left and right edges of the upper part of W nanodisks. The electric field distribution indicates the excitation and near-field coupling of the LSPRs generated by the gap between adjacent W nanodisks.[22–24] Incident light is coupled to the TiN–W nanodisk arrays by exciting PRC and LSPRs, which then excites PSPRs in the bottom W film layer. Therefore, PRC mode and LSPRs are responsible for the high absorption, and the excited PSPRs further enhance the absorption.[22]

Figures 3(c) and 3(d) show the distribution of electric field and magnetic field at 566 nm in the back incidence under the TM polarization. It can be seen that the intensity of the electric field in the front-sided incidence is 3 times stronger than that of the back-sided case, which contributes to the decrease of absorptivity in the back-sided case. Simultaneously, according to the distributions of electric field and magnetic field, it is obvious that the physical mechanism of the broadband absorber in back-sided incidence is the same as that in the front-sided incidence. The difference is that the enhanced electric field is mainly located in the gap of W nanodisks, especially near the upper, lower, and left edges of the nanodisks, while the electric field intensity is not strong in the upper of TiN nanodisks.

4. Results and discussion

To further analyze the influence of geometric parameters on the absorption performances, the absorption characteristics of the thickness tolerance are shown in Fig. 4. The grating period Λ is maintained at 210 nm, the radius of the TiN nanodisk is set to 50 nm, and the radius of the W nanodisk is set to 75 nm. As shown in Figs. 4(a) and 4(b), when the thickness of the SiO_2 layer increases from 40 nm to 140 nm, the bidirectional absorption spectrum widths in the front- and back-sided incidence are both unchanged. However, the bandwidth with high absorptivity shifts to long-wavelength in the visible wavelength range, which can conclude that the thickness of the SiO_2 layer can improve the absorptive efficiency in the long-wave spectrum.

Figures 4(c) and 4(d) exhibit the absorption spectra of the W film when the thickness of the W film increases from 5 nm to 15 nm. It can be clearly seen that in the range of 400 nm–800 nm, the absorption spectrum bandwidth in the front- and back-sided incidence are basically unchanged as the thickness of the W film increases. However, the absorptivity is higher in the range of 460 nm–560 nm when the thickness of W film is 5 nm. Figures 4(e) and 4(f) compare the absorption spectra when the thickness of W disk increases from 250 nm to 350 nm, respectively. It is evident that the absorption spectral bandwidth in the front- and back-sided incidence are both unaffected by the thickness of W nanodisk. Simultaneously, the absorptivity increases gradually in the visible wavelength range.

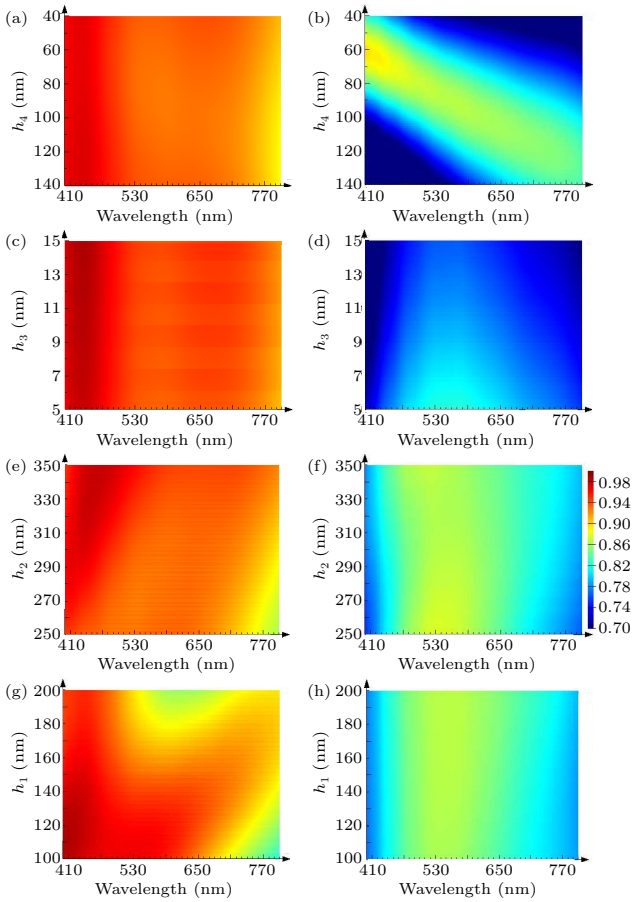


Fig. 4. Panels (a) and (b) are absorption spectra versus with different values of h_4 at the front- and back-sided incidence, respectively. Panels (c) and (d) are absorption spectra versus with different values of h_3 at the front- and back-sided incidence, respectively. Panels (e) and (f) are absorption spectra versus with different values of h_2 at the front- and back-sided incidence, respectively. Panels (g) and (h) are absorption spectra versus with different values of h_1 at the front- and back-sided incidence, respectively.

The absorption spectra are shown in Figs. 4(g) and 4(h) when the thickness of TiN nanodisk increases from 100 nm to 200 nm. We can see that in the range of 400 nm–800 nm, the absorption spectral bandwidth ($A > 89\%$) is still basically unchanged with the front-sided incidence when the thickness of TiN nanodisk increases, but the absorptivity increases. Meanwhile the absorption bandwidth ($A > 70\%$) is basically un-

changed, the spectral absorptivity in the visible range increases gradually in the back-sided case.

In addition, the angle dependence of the front- and back-sided incidence is calculated. Figure 5 shows the results of the incidence angle of light varying from 0° to 30°. When the incidence angle is no more than 30°, the absorption characteristics of front- and back-sided incidence are basically unchanged. Obviously, the absorption properties are almost the same over a relatively wide range of incident angles.

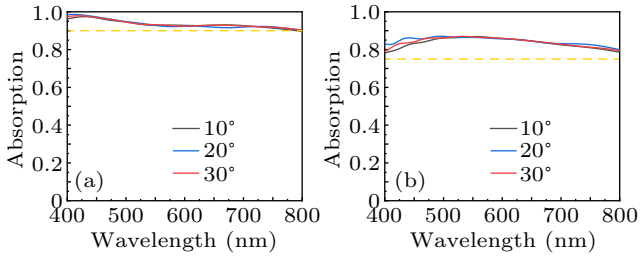


Fig. 5. Absorption spectra verse with different incident angles for the front- (a) and back- (b) sided incidence.

5. Conclusion

A bidirectional broadband absorber in the visible range is demonstrated by using the FDTD method. With the combined effect of LSPRs, PRC mode, and PSPRs, the average absorption of the absorber exceeds 89% at the visible range with the front-sided incident. Illumination from the opposite direction results in absorption of more than 75%. Furthermore, the absorber also exhibits excellent polarization-independence performance and high angular tolerance for bidirectional incidence. The absorber presented in this paper can be employed in a potential application such as solar cells.

Acknowledgments

Project supported by the National Key Research and Development Program (Grant No. 2022YFB2804602) and Shanghai Pujiang Program (Grant No. 21PJD048).

References

[1] Landy N I, Sajuyigbe S, Mock J J, *et al.* 2008 *Phys. Rev. Lett.* **100** 207402
[2] Zhou W X, Shen Y, Hu E T, *et al.* 2012 *Opt. Express* **20** 28953
[3] Khodasevych I E, Wang L, Mitchell A, *et al.* 2015 *Adv. Opt. Mater.* **3** 852
[4] Liang Q, Wang T, Lu Z, *et al.* 2013 *Adv. Opt. Mater.* **1** 43
[5] Lee K T, Ji C and Guo L J 2016 *Appl. Phys. Lett.* **108** 59
[6] Lee K T, Seo S, Lee J Y, *et al.* 2015 *Adv. Mater.* **26** 6324
[7] Yang C, Ji C, Shen W, *et al.* 2016 *ACS Photonics* **3** 590
[8] Yan M, Dai J and Qiu M 2014 *J. Optics* **16** 218
[9] Watts C M, Liu X and Padilla W J 2012 *Adv. Mater.* **24** OP98
[10] Roszkiewicz A and Nasalski W 2012 *Opt. Lett.* **37** 3759
[11] Hedayati M K, Javaherirahim M, Mozooni B, *et al.* 2011 *Adv. Mater.* **23** 5410
[12] Tang J, Zhou Y, Liu N, *et al.* 2020 *Appl. Phys. Express* **13** 064001
[13] Shen S, Tang J, Yu J, *et al.* 2019 *Opt. Express* **27** 24989
[14] Cheng X G, Zhen S W, Jing B, *et al.* 2019 *Chin. Phys. B* **28** 024203
[15] Palik E D 1998 *Handbook of Optical Constants of Solids* (New York: Academic Press) p. 3
[16] Xin B H, Bing W, Kai H F, *et al.* 2019 *Chin. Phys. B* **28** 074102
[17] Hu J H, Wang J G, Nie Y F, *et al.* 2019 *Chin. Phys. B* **28** 100201
[18] Wei B, He Q, Li J, *et al.* 2011 *Acta Phys. Sin.* **60** 104102 (in Chinese)
[19] Xu Z S and Ma X K 2012 *Acta Phys. Sin.* **61** 110206 (in Chinese)
[20] Liu J, Chen W, Zheng J C, Chen Y S and Yang C F 2020 *Nanomaterials* **10** 27
[21] Zhou J, Liu Z Q, Liu G Q, Pan P P, Liu X S, Tang C J, Liu Z M and Wang J Q 2020 *Opt. Express* **28** 36476
[22] Lei L, Li S and Huang H 2018 *Opt. Express* **26** 5686
[23] Luo M, Shen S, Zhou L, *et al.* 2017 *Opt. Express* **25** 16715
[24] Feng R, Qiu J, Cao Y, *et al.* 2015 *Opt. Express* **23** 21023